Through-The-Wall Detection with Gated FMCW Signals using Optimized Patch-Like and Vivaldi Antennas

F. Fioranelli, S. Salous, I. Ndip, and X. Raimundo

***Abstract*—This paper presents the design and optimization of patch-like antennas for Through-The-Wall Imaging (TTWI) radar applications in the frequency range 0.5-2 GHz. A basic antenna configuration is analyzed and modified through an optimization aiming at reducing the size of the antenna and at focusing the radiated power in a single lobe to be directed towards the wall and the targets to be detected. Both the basic and the optimized antennas have been manufactured and tested. The optimized patch antennas and a conventional Vivaldi antenna have been successfully used in the frequency modulated interrupted continuous wave (FMICW) radar system developed at Durham University. Results of a novel wall removal technique for through-the-wall imaging using numerical simulations and measurements aimed at the detection of stationary targets and people are presented.**

***Index Terms*— Printed antennas, UWB radar, through-the-wall imaging**

I. Introduction

Techniques for through-the-wall-imaging (TTWI) have been attracting interest from law enforcement agencies and first responders, as they can improve the situational awareness of policemen and soldiers operating in an urban context and support first responders in search and rescue operations. Surveys of possible technologies for through-the-wall detection indicate that microwave ultra wide band (UWB) signals are the most suitable, provided that an effective choice for the frequency range of the waveform is made [1-2]. On the one hand a wide bandwidth is desirable to achieve fine down range resolution while through-wall penetration losses for common wall materials increase with frequency. Thus, a frequency range of 0.5-2 GHz is considered suitable to get good resolution for image formation and good penetration even through thick walls.

In TTWI radar systems, antennas are of fundamental importance to radiate power towards the wall and the targets to be detected. They should have well matched impedance across the wide bandwidth, and radiation patterns suitable to focus most of the energy towards the area to be investigated. Lower operational frequencies provide better through-wall penetration but also imply bulkier antennas. Wide bandwidth provides finer range resolution, but good impedance and suitable radiation patterns for the antennas must be ensured across such bandwidth. Weight and size of the antennas also need to be taken into account, depending on the type of radar system (e.g. handheld or mounted on a vehicle).

Different design models have been proposed in the literature. Antipodal or exponentially tapered Vivaldi antennas are widely used due to their high gain and narrow beam-width, either as single antennas or in array configurations [1, 2]. Vivaldi and linearly tapered slot design may be combined to create a hybrid model [3, 4]. Horn antennas may replace Vivaldi antennas having comparable gain and radiation pattern directivity, although they tend to be bulkier [5-7]. Archimedean spiral antennas have also been used due to their compact size and circular polarization [8, 9]. Elements printed on dielectric substrate are another common choice. Many different shapes are available in the literature, such as simple geometrical squares or ellipses which could be worn directly by users in the field [10], or more elaborate shapes to achieve desirable properties like dual polarization or side lobe suppression [11]. Improved performance can be also achieved using ad hoc designs, for instance the two-flare antenna for detection of people buried under rubble as in [12].

In this paper, we propose a novel patch-like antenna for TTWI applications in the frequency range 0.5-2 GHz. A basic configuration of the antenna has been designed, systematically simulated and manufactured, showing good agreement with the simulated results. Then the antenna has been optimized with the aid of commercial software tools to reduce its dimensions and improve its radiation pattern. The optimized antennas have been used in the TTWI radar system developed at Durham University to confirm the effectiveness of a novel wall removal technique based on gated frequency modulated continuous wave signals when detecting stationary targets and people moving behind walls. This approach is implemented for the first time in the through-wall imaging field for the suppression of wall reflection signals and has been also validated through numerical simulations using CST Microwave Studio. To the best of our knowledge, the use of

Francesco Fioranelli, Sana Salous, and Xavier Raimundo are with the Centre for Communications Systems, School of Engineering and Computing Sciences, Durham University, South Road, DH1 3LE, Durham, UK (e-mail: sana.salous@durham.ac.uk).

Ivan Ndip is with the Fraunhofer Institut für Zuverlässsigkeit und MIkrointegration, Fraunhofer IZM, Gustav Meyer Allee 25, 13355, Berlin, Germany (e-mail: Ivan.Ndip@izm.fraunhofer.de).

this commercial software for realistic three-dimensional simulations of TTWI scenarios using frequency modulated continuous wave (FMCW) waveforms is also novel, given the non-trivial implementation of FMCW signals in CST and the computational burden related to these scenarios. Two algorithms usually used in medical imaging have been adapted to create through-wall radar images using the simulated and experimental data, namely delay-sum-integration (DSI) and delay-multiply-sum-integration (DMSI), and results compared with the more conventional back projection (BP) algorithm. In the experimental campaign both optimized patch and conventional Vivaldi antennas have been used, showing that the proposed antennas detect less clutter and undesired signals, simplifying the application of the proposed wall removal technique. Besides suppression of undesired antenna cross-talk and wall reflections with the novel approach, our TTWI system can achieve through-wall detection of stationary objects and moving people using the simpler and cheaper proposed patch-like antennas in comparison with other designs implemented in the literature. Horn antennas [5-7] are more expensive to buy and bulkier when deployed in an actual system. Exponential [1] and linear tapered slot antennas [13] tend to be larger when operating at low frequencies such as 0.5 GHz to provide good through-wall penetration. The proposed antenna is also easy to design and manufacture, and made of inexpensive FR4 substrate.

This paper is organized as follows. In section II the basic and the optimized configurations of the patch-like antenna are presented, with comparisons of simulated and measured results for the S11 parameter and gain radiation patterns. Section III describes the Vivaldi antenna which was designed and manufactured to compare with the proposed optimized patch antennas. In section IV examples of numerical simulations for through-wall detection of stationary targets are briefly presented, followed in section V by some results from the experimental campaign performed using the developed antennas and radar system. Finally section VI concludes this paper.

II. The Patch-Like Antenna

A. The basic antenna configuration – Simulation, fabrication, and measurements

The basic antenna design consists of a rectangular patch fed by a microstrip line printed on common FR4 dielectric substrate, with a ground plane on the other side of the substrate. The thickness of the dielectric and of the copper layers is 1.5 mm and 80 μm, respectively. Prior to manufacturing, the antenna was extensively simulated with the software ANSYS HFSS to get its S11 parameter below -10 dB across the desired frequency range 0.5-2 GHz, while keeping the overall size as small as possible. All the HFSS simulations used the discrete sweep mode with 50 MHz steps across the bandwidth. The maximum delta in terms of change in the magnitude of the S-parameters between two consecutive mesh refinement steps was set at 0.001, with at least three steps below this threshold for increased convergence accuracy.

Fig. 1 shows the 3D simulation model of the antenna and the coordinate system, with the long side of the antenna aligned with the Y axis and the short size with the X axis, as well as the manufactured prototype of the antenna with its final dimensions.

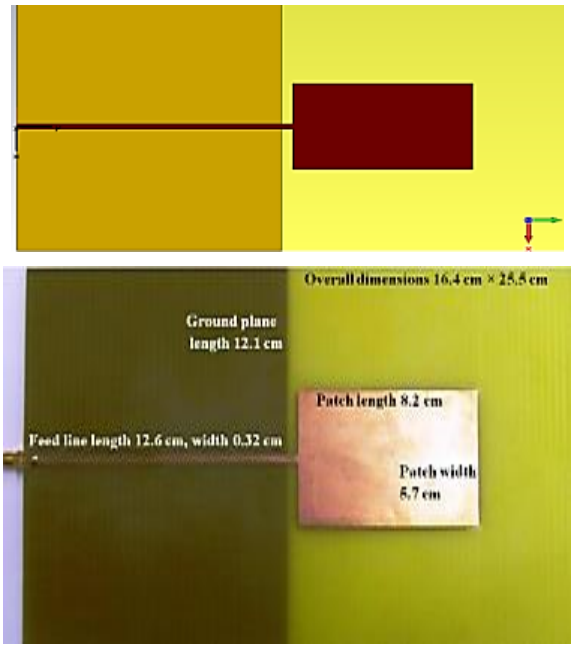

Fig. 1 Simulation model and top view (XY plane) of the manufactured prototype of the basic antenna basic configuration

The return loss of the antenna was measured from the S11 using a calibrated network analyzer in the anechoic chamber at the Fraunhofer IZM. Fig. 2 shows a comparison of simulated and measured data for this parameter. The design was also simulated using CST MICROWAVE STUDIO, which uses a time domain numerical method (Finite Integration in the Time Domain), to compare the results with those from HFSS, which uses a frequency domain method (Finite Elements Method). The former method can provide the broadband frequency response of the antenna under test with a single simulation followed by FFT, whereas the latter method requires the resolution of a large system of equations for each frequency point of the bandwidth under test [14]. A time domain method may therefore be faster to characterize the broadband antennas proposed in this paper, even if the required computational time depends on the available system. In this case the additional time required by the frequency domain method to simulate many frequency points was compensated by running the software HFSS on a cluster of computers. This led to a computational time of a few hours, which is comparable with the time required by CST running on a single workstation. The S11 is below the -10 dB threshold across the desired frequency range 0.5-2 GHz, and there is good similarity between measurements and numerical simulations. The offset between simulated and experimental data for the lower resonance peak may be due to the tolerances in manufacturing the antenna, in particular the discrepancies between the simulated SMA connector and the actual position and soldering of the connector for the manufactured antenna.

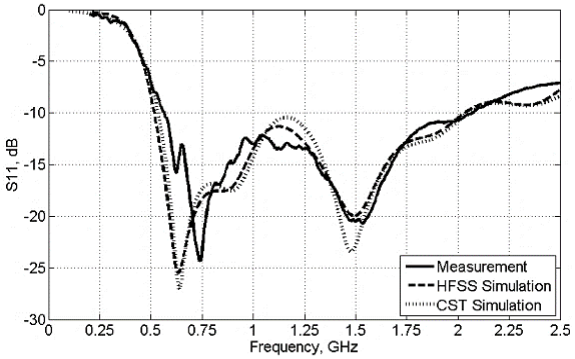

Fig. 2 Measured and simulated S11 of the basic antenna configuration

The radiation patterns of the antenna have been measured in the azimuth plane at θ equal to 90° (XY plane) and in one of the elevation planes at φ equal to 0° (XZ plane), which are the most important to characterize for this antenna (the other elevation plane YZ or φ equal to 90° is not considered). We used the gain-transfer method to derive the gain of the antenna under test (G_{AUT}) from measurements of the transmitted power with another antenna with well-known and calibrated gain (G_{ST}), the so-called gain-standard antenna [15]. The gain in dB can be computed as in (1):

$$G_{AUT} = S_{21} - G_{ST} + 20Log(\frac{4\pi R}{\lambda}) \quad (1)$$

where the transmitted power is the broadband S21 parameter from the network analyzer, R is the distance between the antennas (typically 1 m), and λ is the wavelength. A calibrated horn was used as gain-standard antenna across the 1-2 GHz bandwidth, whereas a calibrated log-periodic antenna was used for the lower desired frequencies. The method assumes free space and antennas placed in the far-field during the measurement. The first condition is satisfied by performing the measurements in the anechoic chamber. For the second condition we can calculate the far-field distance $2D^2/\lambda$. Given the larger dimension of the horn equal to 24.4 cm, this distance is 38.4 cm and 76.8 cm, at 1 GHz and 2 GHz respectively, so that the far-field condition is fulfilled with 1 m spacing between the antennas. When using the log-periodic antenna with length approximately 60 cm, the far-field distance is longer than 1 m and the measured gain is lower than the actual far-field gain because of the remaining near-field components and the non-uniform illumination of the antenna under test. This error is expected to be less than 1 dB [15] and therefore does not compromise the suitability of the proposed antenna for TTWI applications. In order to measure the total gain of the antenna under test, the partial gains from both linear vertical and linear horizontal polarizations are measured and then added together for each plane. This can be done by performing two partial gain measurements using a single linearly polarized gain-standard antenna (in our case either the horn or the log-periodic), which is rotated by 90° to achieve two orthogonal polarizations. The total gain is then normalized and compared with the results from numerical simulations.

Fig. 3 shows the gain radiation patterns for the patch-like antenna at 1 GHz and 2 GHz in the aforementioned planes. Good agreement in the shape of the patterns can be seen comparing simulations with measurements. In the azimuth plane the antenna radiates two lobes in the direction 60° and 120°, and this pattern becomes more directional as the frequency increases, as expected. This two-lobe pattern may cause problems for TTWI applications, since the radiated power cannot be clearly focused towards the wall and the targets. Even if one of the lobes is focused, clutter and undesired signals may be received through the other lobe in case of monostatic scenario with a single antenna working at the transmitter and at the receiver at the same time, or strong cross-talk may occur between different antennas in case of scenarios where multiple antennas are used.

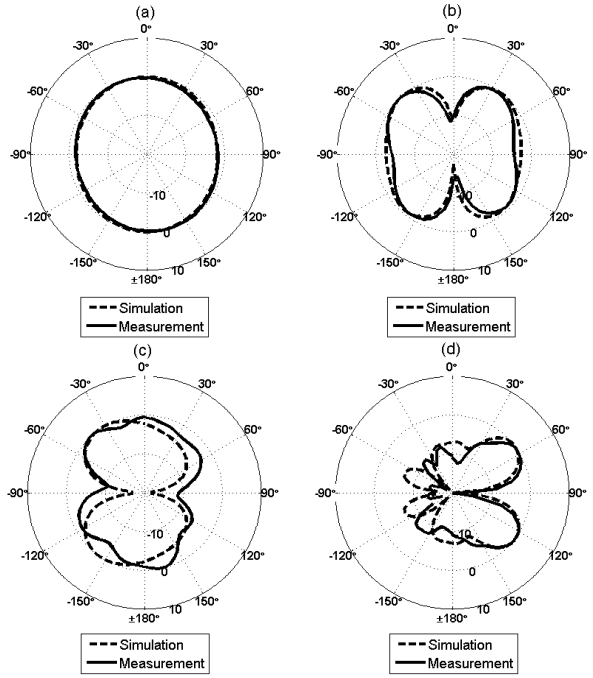

Fig. 3 Normalized total gain patterns for the basic antenna configuration: (a) elevation plane XZ at 1 GHz, (b) elevation plane XZ at 2 GHz, (c) azimuth plane XY at 1 GHz, and (d) azimuth plane XY at 2 GHz

B. The optimized antenna configuration – Simulation, fabrication, and measurements

To focus the beam of the patch-like antenna presented in the previous section for TTWI applications, an additional ground plane strip is added to suppress one of the radiating lobes in the azimuth plane and increase the gain in the direction of the remaining lobe. The overall size was further reduced and the patch width and length modified so that the resulting resonance peaks maintain the impedance matched across the desired 0.5-2 GHz bandwidth. This optimization has been performed with commercial software tools taking into account all the parameters involved, such as patch length and width, feed line sizes, ground plane length, ground plane strip width, and additional patch size.

Fig. 4 shows the manufactured optimized antenna with its final dimensions. The overall dimensions are 14 cm x 17 cm against 16.4 cm x 25.5 cm of the patch-like prototype. On the lower side of the substrate a metal patch was also added to

improve the impedance matching as can be seen in Fig. 5a, showing the simulated S11 of the antenna with and without this small patch.

Fig. 4 Top view of the optimized patch-like antenna and its dimensions (long side of the antenna aligned with the Y axis and the short size with the X axis)

Fig. 5b compares the S11 of the optimized configuration for simulations using HFSS and CST with measured data from the manufactured antenna. The curves follow a similar pattern, even though the manufactured prototype presents resonance peaks which are slightly shifted in comparison with the simulations, probably because of tolerances in the manufacturing process when soldering the SMA connector. The antenna is matched across the desired bandwidth, with S11 below the usual -10 dB threshold.

Fig. 6.a presents the CST simulated input impedance of the proposed antenna while Fig. 6.b presents the coupling between the two proposed optimized-patch antennas with different spacing distances from 10 cm to 30 cm. The antennas are oriented in side-by-side configuration, as shown in Fig. 17 later in the paper. It can be seen from both the CST simulation and actual measurements that the coupling is below 15 dB for antenna separation equal to 20 cm (the value used for the experimental campaign discussed in section V) or higher. The undesired signal given by the coupling between the transmitter and receiver antenna can be mitigated/removed in through-wall radar applications by applying the proposed gated FMCW signals.

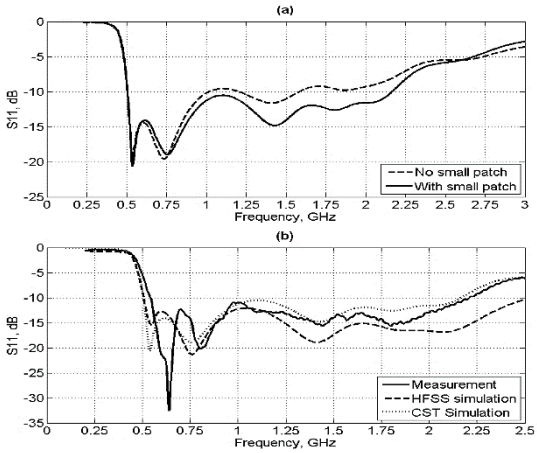

Fig. 5 Simulated S11 of the optimized patch-like antenna with and without small patch (a), and measured and simulated S11 of the optimized patch-like antenna (b)

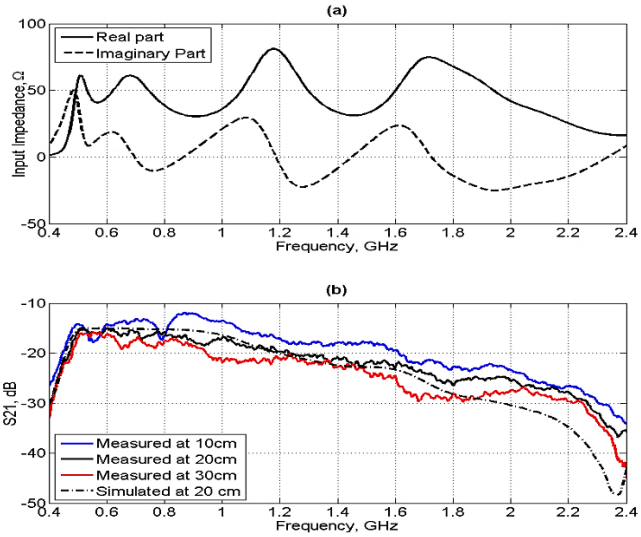

Fig. 6 Simulated input impedance of the optimized patch like antenna (a), and simulated and measured mutual coupling of 2 optimized patch-like antennas at different spacing distance (b)

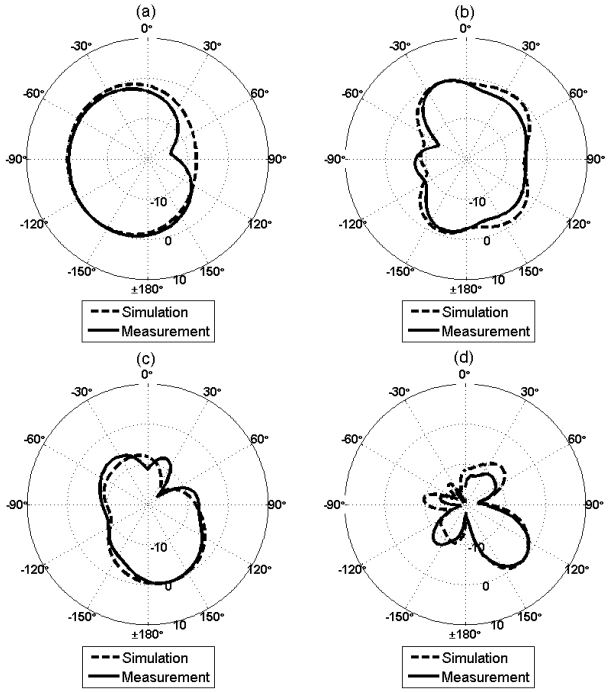

Fig. 7 Normalized total gain patterns for the optimized antenna configuration: (a) elevation plane XZ at 1 GHz, (b) elevation plane XZ at 2 GHz, (c) azimuth plane XY at 1 GHz, and (d) azimuth plane XY at 2 GHz

Fig. 7 shows the normalized gain radiation patterns for the optimized patch-like antenna at 1 GHz and 2 GHz in the elevation plane φ equal to 0° and azimuth plane θ equal to 90°. Good agreement between simulations and measurements is achieved, as well as beam focusing in a single radiating lobe in the azimuth plane in the direction of roughly 130°-150°.

Fig. 8 presents the simulated co-polarized and cross-polarized 3rd Ludwig components at 1 GHz and 2 GHz in the elevation plane φ equal to 0° and azimuth plane θ equal to 90°. The possibility of exploiting cross-polarized components for wall mitigation and through-wall detection of human beings has been highlighted in [16]. However the analysis of issues such

as antenna polarization purity and effective reception of weak cross-polarized components when developing an actual cross-polarized radar system is beyond the scope of this paper.

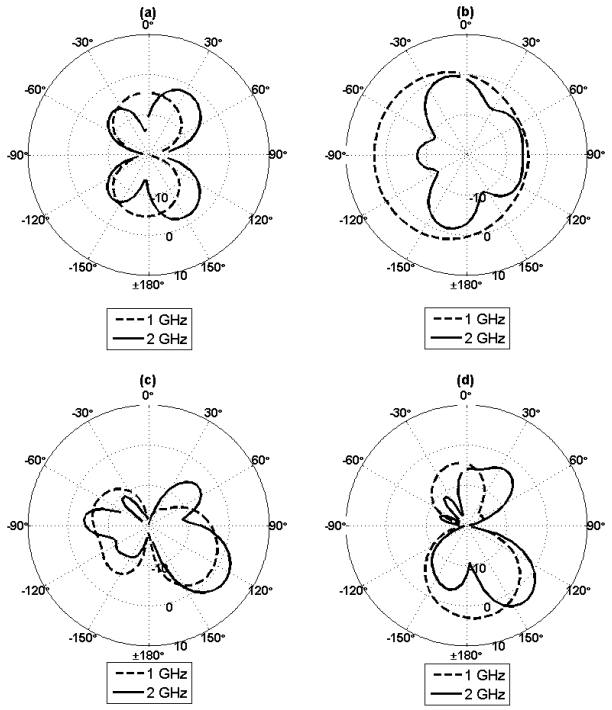

Fig. 8 Simulated 3rd Ludwig components for the optimized antenna configuration: (a) cross-polar component in the elevation plane XZ, (b) co-polar component in the elevation plane XZ, (c) cross-polar component in the azimuth plane XY, and (d) co-polar component in the azimuth plane XY

III. The Vivaldi Antenna

An alternative antenna has been developed at Durham University to perform through-wall experiments. It is a conventional antipodal Vivaldi designed to work across the desired bandwidth 0.5-2 GHz. Fig. 9 shows the 3D simulation model of this antenna, with the long side aligned with the X axis and the short side with the Y axis. The antenna has been simulated using both the time domain and the frequency domain solver of CST Microwave Studio, and then manufactured on substrate Taconic CER10 with 1.5 mm thickness. This substrate has been chosen for its higher permittivity (ε_r equal to 10 with ±5% tolerances) compared with FR4, in order to keep the antenna size relatively small while working at low frequencies starting at 0.5 GHz to achieve good through-wall penetration. Its S11 parameter has been measured with a network analyzer at Durham University. The overall dimensions of this antenna are 26 cm × 18.5 cm.

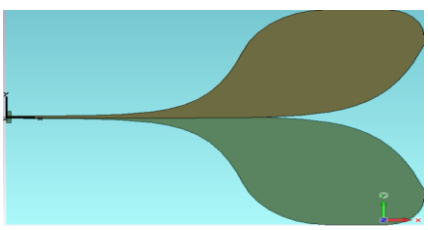

Fig. 9 Simulation model of the Vivaldi antenna with coordinate system

Fig. 10 compares the simulated and measured S11 parameter of this antenna, showing similar patterns apart from the slight shift of the resonance peaks for the manufactured antenna, which does not compromise the matching across the desired bandwidth. Fig. 11 shows the normalized gain radiation patterns at 1 GHz and 2 GHz in the elevation plane φ equal to 0° and azimuth plane θ equal to 90°.

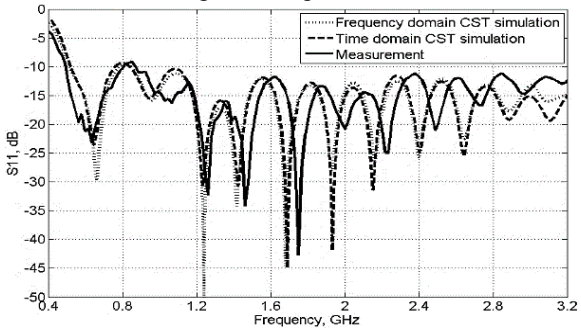

Fig.10 Measured and simulated S11 of the antipodal Vivaldi antenna

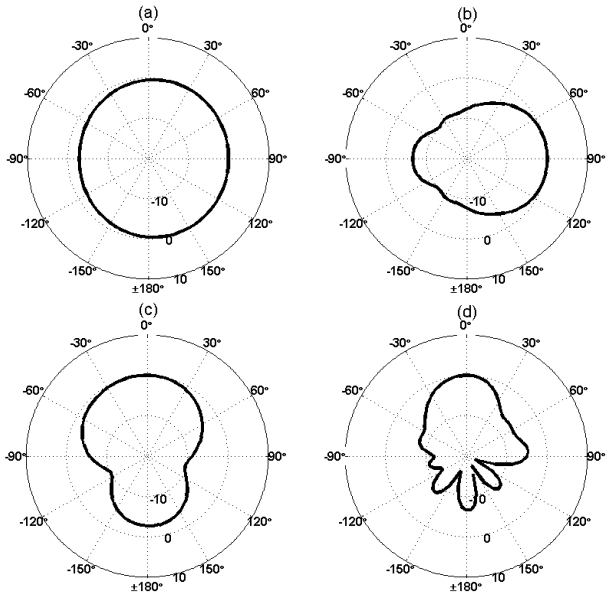

Fig. 11 Normalized total gain patterns for the Vivaldi antenna from simulations: (a) elevation plane XZ at 1 GHz, (b) elevation plane XZ at 2 GHz, (c) azimuth plane XY at 1 GHz, and (d) azimuth plane XY at 2 GHz

The Vivaldi antenna is bigger than the optimized patch (26 cm × 18.5 cm against 17 cm × 14 cm) and made of a more expensive substrate. Both antennas present S11 parameter lower than -10 dB across the desired 0.5-2 GHz bandwidth; the Vivaldi is matched even at a higher frequency up to 3 GHz, which could be useful for further future measurements with wider bandwidth to increase the resolution. Even if both antennas have a main lobe in the radiation pattern in the azimuth plane, the optimized patch has a narrower lobe and presents smaller side lobes. This would benefit the through-wall measurements as the radiated power would be more focused towards the target area and less undesired signals as wall reflections would be received. Fig. 12 presents the simulated total gain in the direction of maximum radiation as a function of frequency for the antennas discussed in this paper. For both the Vivaldi and the optimized-patch the gain varies

across the desired bandwidth between 2 and 7 dB. Other reported UWB printed antennas for TTWI or similar imaging applications provide comparable values of gain, for example 5 dB [17] , 4 dB [18], 2-6 dB [19], and 8 dB [11].

In [22] we showed that the patch antenna is still usable when placed at 10 cm from walls, with some minor degradation of its performance. In Fig. 13 we compare the measured S11 of the patch and Vivaldi antenna when they are placed at different distances from the brick wall used for the experimental results presented in this paper. We can see that there is degradation, especially for the Vivaldi antenna, when the antennas are physically touching the wall, but they are still usable at short stand-off distances such as about 5 cm.

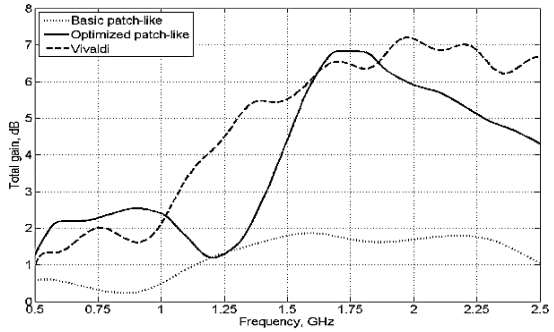

Fig.12 Total gain as a function of frequency of the presented antennas

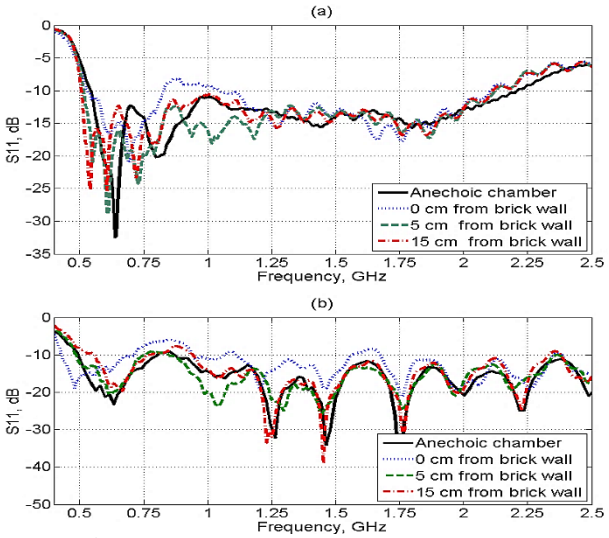

Fig. 13 S11 of the optimized patch (a) and Vivaldi (b) antennas measured at different distances from the brick wall

IV. Numerical Simulations of TTWI Scenarios

Numerical simulations have been performed to investigate the effectiveness of a novel wall removal technique based on gated frequency modulated continuous wave (FMCW) signals, also called frequency modulated interrupted continuous wave (FMICW). These techniques aim at mitigating/removing the undesired contribution of wall reflections from the received signal of radar systems for TTWI. Wall reflections can compromise the detection performance as they are significantly stronger than echoes of the desired targets and they can saturate and block the receiver [20]. FMICW signals have been previously used in monostatic ionospheric channel sounding and ocean surface sensing, but to the best of our knowledge its use as wall removal approach in TTWI is novel. With this technique, the transmitter and the receiver of a normal FMCW radar system are switched on and off with complementary gating sequences. The effect of this gating operation on the overall received power can be investigated through the mean received signal (MRS), which is the cross-correlation between the sequence applied at the transmitter and the complementary sequence applied at the receiver. Assuming to model the gating sequences as binary on-off functions, the MRS depends on properties such as number of bits and bit duration, and on the round-trip delay to the targets. An exhaustive analysis of FMICW waveforms and possible gating sequences is provided in [21]. The MRS can be considered as a weight applied to the received power of the radar, thus providing additional attenuation at some values of round-trip delay called blind ranges. For TTWI applications it is possible to design suitable sequences which provide attenuation at values of round-trip delay corresponding to the undesired wall reflections, and no or little additional attenuation at delays corresponding to the area under test. In a real scenario the stand-off distance between wall and radar system is generally known or measurable, so the user can choose a gating sequence providing a blind range at such distance and then progressively tune its parameters to optimize the wall removal performance. This optimization is scenario dependent as the duration of the undesired wall reflection signal depends on the wall electrical parameters and internal structure. For instance in the case of thick walls with internal air gaps, the user may need to choose gating sequences providing a very long blind range to achieve effective wall removal and target detection enhancement.

A detailed discussion of advantages and disadvantages of existing wall removal techniques and proposed FMICW waveforms can be found in [22, 23], together with a comprehensive review of TTWI radar systems based on different waveforms. For instance, a time-gating device at the front-end of the receiver could suppress the wall reflection, but apart from its hardware complexity and related costs, it would be applicable only to pulse-based systems and not to systems based on frequency modulated waveforms. Our focus is on these systems, as they generally require less expensive Analogue to Digital Converter at the receiver and lower transmitted peak power. On the other hand, the post-processing approach of cutting or zero-padding the undesired contributions in the received signal after digitization would not address the problem of reduction of the receiver dynamic range and sensitivity [24].

The simulations presented in this work have been performed using CST Microwave Studio and its finite integration in the time domain (FIT) method, which is suitable for large and detailed structures like realistic through-wall scenarios. Our scenarios are three-dimensional rooms with 4-5 m^2 area and 15 cm thick walls, plus ceiling and floor. These rooms contain a metallic cabinet, which is a target with high radar cross section (RCS) and a human phantom with lower RCS. The real and imaginary skin permittivity parameters in

CST at the center frequency 1.25 GHz are 31.29 and 115.239, respectively. A material with the same electrical parameters of human skin is used to model uniformly the phantom, without the internal tissues and organs. This is possible because it has been observed that most of the electromagnetic energy at the frequency used for TTWI is reflected by the skin without penetration into the body [16, 25]. This simplified human phantom allows saving memory and CPU time resources. An FMICW signal with bandwidth 0.5-2 GHz has been used, providing 10 cm range resolution. The electromagnetic field is sampled at 9 probes which simulate the presence of an array of receiving antennas. The probes are placed 25 cm apart, thus forming a 2 m long array.

The signals recorded at the probes are processed with three algorithms to create radar images: back projection (BP) which is a well-known imaging algorithm [26], delay-sum-integration (DSI) and its variant delay-multiply-sum-integration (DMSI) originally developed for breast cancer detection [27, 28] and not used for through-wall detection.

The pixel intensity for the BP algorithm can be written as in (2):

$$I(x_i, y_j) = \sum_{k=1}^{N} E_k(\tau_{ijk}) \tag{2}$$

where the indices *(i,j)* denote the coordinates of the pixels, and E_k denotes the received signal at the k^{th} transmitter-receiver pair; τ_{ijk} is the round-trip delay. The pixel intensity for the DSI and the DMSI algorithms is given in (3) and (4) respectively:

$$I(x_i, y_j) = \int_0^W \sum_{k=1}^{N} E_k(t - \tau_{ijk})dt \tag{3}$$

$$I(x_i, y_j) = \int_0^W \sum_{k=1}^{N-1} \sum_{l=k+1}^{N} E_k(t - \tau_{ijk}) E_l(t - \tau_{ijl})dt \tag{4}$$

where in (4) the indices k and l denote which receivers are involved in the multiplication in pairs, and τ_{ijk} and τ_{ijl} are the round-trip delays related to each received signal. Compared with BP, the main difference is the use of the integration window W to generate the pixel intensity, rather than just picking a single value of the received signal at the corresponding round-trip delay. More details and a comparative analysis of these algorithms can be found in [27, 29].

Accurate values of the round-trip delay related to the transmitter-pixel-receiver propagation path are necessary to avoid displacement and blurring in the radar images when applying these algorithms. In comparison with a free space scenario, electromagnetic waves are slowed down while propagating through the wall, so that an additional correction factor should be added to the estimation of the round-trip delay. This correction is directly proportional to the permittivity of the wall material and to the length of the through-wall propagation path. We estimate this length through a simplified approach which neglects the refraction at the wall-air interface caused by the permittivity contrast ("straight ray approximation"). This provides good results and allows avoiding transcendental equations which would be involved in the exact solution of this problem [30]. The permittivity of the wall material and the wall thickness are known from CST for our simulations.

Fig. 14a shows a view of the first simulated scenario presented in this paper, where the green points on the left-hand side represent the probes. The room size is 235 cm × 200 cm and its walls are made of 1 year old concrete with real relative permittivity 5.657 and imaginary part 0.198 at 1.25 GHz, and are 15 cm thick. The stand-off distance of the wall from the probes is 250 cm. A 5 cm air gap is placed in the middle of the wall to make it more realistic, as well as more challenging for the detection of the targets as this structure can trap electromagnetic waves, thus increasing the duration of the wall reflection signal [31]. Fig. 14b illustrates the second scenario, where a 10 cm thick partition wall with a wooden door (brown box) is inserted in the middle of the room to separate two human phantoms. The stand-off distance of the probes from the 15 cm thick external wall is 25 cm. The walls are made of 40 years concrete with real permittivity 4.642 and imaginary part 0.352 at 1.25 GHz. The detection of the phantom behind the partition wall is particularly challenging.

Fig. 15 presents images obtained using normal FMCW signals and the proposed FMICW signals, with different imaging algorithms, for the first scenario. The color scale is the same for every sub-figure. Both targets can be detected with the proposed FMICW waveforms, whereas only wall reflections appear in the image if normal FMCW signals are used. With the same dynamic range from the maximum, the DMSI image appears to contain less clutter and provide the radar user with a more precise indication of the actual target positions in the area under test. Fig. 16 presents images using FMCW and different FMICW waveforms for which the parameters of the gating sequences are progressively adapted to mitigate the reflections from both the external wall and the partition wall and to detect both human phantoms. During this adaptation process the gating sequence is changed from a 3 bit M-sequence to a square wave, and their bit duration and duty cycle optimized to achieve good wall removal for this particular scenario. Every sub-figure is created using the BP algorithm and has the same color scale. Only reflections from the exterior and from the partition wall can be detected if normal FMCW waveforms are used, as in figure 16a. In figure 16b the blind range of the gating sequence (in this case an M-sequence) removes only the reflection from the external wall, whereas in figure 16c the gating sequence (in this case a square wave) removes only the partition wall. In figure 16d a modified square wave is used so that two blind ranges are provided to mitigate the contribution from the external wall and to remove the partition wall.

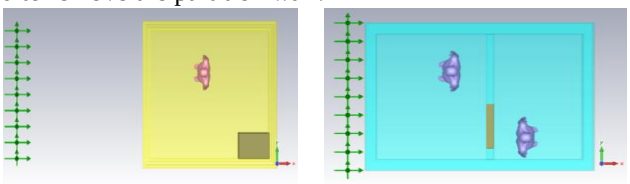

Fig. 14 View of the first and second simulated scenarios with probes and targets inside the room, respectively on the left and right-hand side

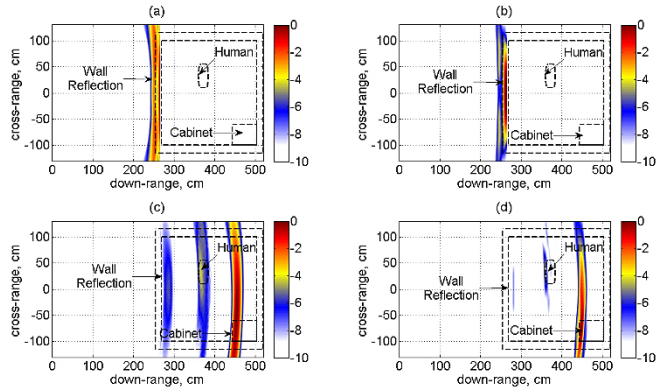

Fig. 15 Radar images in log scale for the first scenario: (a) using FMCW and BP algorithm, (b) using FMCW and DMSI algorithm, (c) using FMICW and BP algorithm, and (d) using FMICW and DMSI algorithm

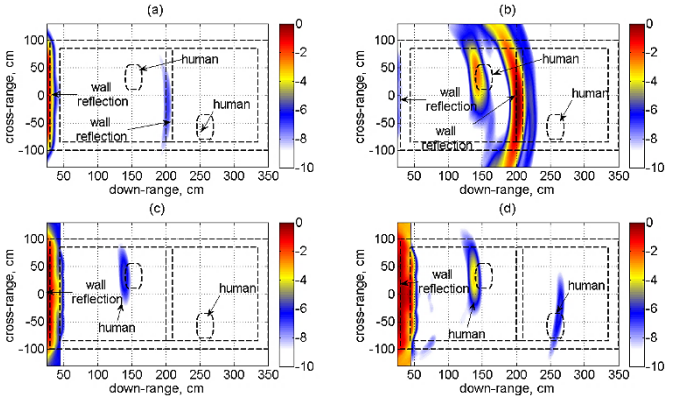

Fig. 16 Radar images in log scale using the BP algorithm for the second scenario: (a) using FMCW waveforms, (b) using FMICW with M-sequence, (c) using FMICW with square wave, and (d) using FMICW with modified square wave

V. Experimental Results for Realistic TTWI Scenarios

An experimental campaign has been performed in realistic environments at the School of Engineering and Computing Sciences, Durham University, to validate the proposed FMICW technique. Two optimized patch-like antennas have been used at the transmitter and at the receiver of the radar system developed for these experiments. This system is based on arbitrary waveform generators (AWG) to create FMICW signals and to change flexibly waveform parameters such as bandwidth, duration, and type and features of the gating sequences. The system has 1.5 GHz bandwidth and signal duration 400 μs, corresponding to 10 cm range resolution and ±1250 Hz unambiguous Doppler coverage.

The Doppler resolution depends on the duration of the acquired data, in our case 0.1 Hz for 10 s of processed data. The transmitted power is 28 dBm and the system is able to successfully detect echoes after 90-100 dB attenuation, which is a typical value for through-wall radar applications [32, 33].

The experiments aimed at the through-wall detection of several stationary objects in two different environments. In the first scenario the targets are placed inside a meeting room with office-like pieces of furniture (wooden chairs and tables, computers and monitors). The wall is 8 cm thick and made of plastered plywood panels, with honeycomb cardboard layer inside. In the second scenario the targets are placed on an open landing behind a 16 cm thick wall made of plastered bricks. Homogeneous structure and relative permittivity is assumed for simplicity for both walls, with values 1.6 for the hollow plywood wall and 4.6 for the brick wall [20].

The experiments were performed in synthetic aperture radar (SAR) approach. The transmitting and the receiving antennas are placed 20 cm apart and moved along an array of 7 different positions separated by 10 cm. The stand-off distance of the antennas from the wall is about 1 cm. Fig. 17 shows on the left hand-side a possible target and on the right hand-side the antennas and part of the radar system mounted on a trolley on the other side of the brick wall. The experiment was conducted with several metallic and non-metallic targets. The results shown here are for a plastic jerrycan filled with water, which has lower RCS than a metallic target. The antennas were oriented to focus the main lobe of the radiation pattern towards the targets.

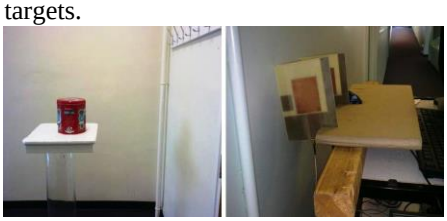

Fig. 17 View of the experimental setup with stationary target on the open landing behind the brick wall

Radar images relating to the plywood wall scenario are presented in figure 18, where every sub-figure has the same color scale. The effectiveness of the proposed wall removal technique can be seen by comparing the images obtained using normal FMCW signals (Fig. 18a) with those obtained using FMICW waveforms. In the former case only wall reflections are detected in the image, whereas in the latter case these undesired contributions are removed by the blind range of a suitable gating sequence, thus allowing the correct detection of the target. Comparing the results from different imaging algorithms with the same dynamic range, DMSI images provide a more precise indication of the actual target positions. Similar results were obtained for the metallic tin in Fig. 17 and for other targets.

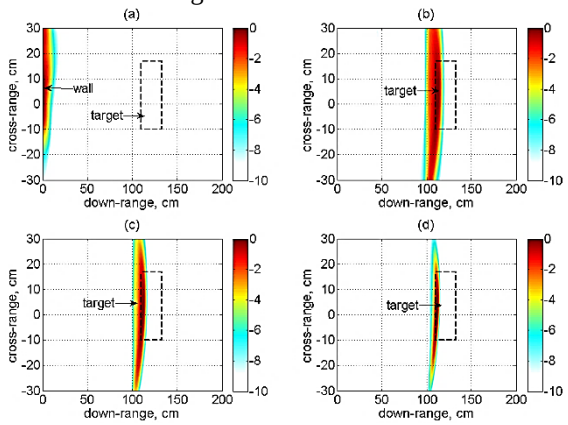

Fig. 18 Radar images in log scale for the plastic jerrycan filled with water behind plywood wall: (a) using FMCW and BP algorithm, (b) using FMICW and BP algorithm, (c) using FMICW and DSI algorithm, and (d) using FMICW and DMSI algorithm

Figure 19 present results related to the scenario with brick wall, comparing images obtained with FMCW and FMICW signals and using the BP and the DMSI algorithm. The effectiveness of the proposed FMICW waveforms and the better performance of the DMSI algorithm in comparison with the BP are demonstrated also in this scenario with a more challenging wall, which is thicker and has higher permittivity. This produces wall reflections which extend longer along the range direction, as it can be seen comparing sub-figures 19a with and 18a. Therefore the parameters of the gating sequence for FMICW signals were adapted to the brick wall in order to provide longer blind ranges.

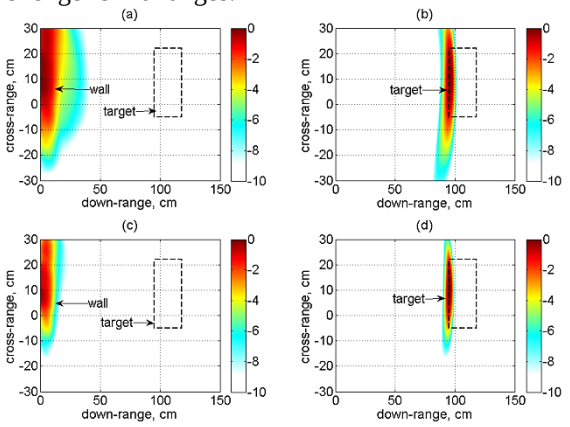

Fig. 19 Radar images in log scale for the plastic jerrycan filled with water behind brick wall: (a) using FMCW and BP algorithm, (b) using FMICW and BP algorithm, (c) using FMCW and DMSI algorithm, and (d) using FMICW and DMSI algorithm

The radar system and the wall removal technique based on gated FMCW signals have been also successfully tested in case of detection of people walking behind walls. The detection is performed through the computation of the Delay-Doppler pattern via double FFT processing [34]. The Doppler shift caused by the motion of the moving target is extracted from the data and shown as colored spots, with the Doppler values proportional to the speed of the target and the delay values proportional to the distance of the target from the radar system during the measurement. In these experiments the person was walking back and forth on a radial trajectory, which generates a Doppler signature which is both positive and negative, indicating that the target is going closer to and farther from the radar system. Initially FMCW signals are used and profiles of the received power as a function of delay/range are extracted to detect the contribution of wall reflections. This allows the user to design a suitable gating sequence to mitigate/remove this undesired signal and enhance the detection of the Doppler caused by the target. These experiments have been performed in the aforementioned scenario with brick wall, but also in a new teaching room presenting a 25 cm thick wall made of concrete blocks, which is quite challenging for through-wall detection. Both the optimized patch and the antipodal Vivaldi antennas have been used in these experiments.

Fig. 20a-20b and 21a-21b compare respectively the delay profiles and the Delay-Doppler for the brick wall scenario, when the two different antennas are used. Fig. 20c-20d and 21c-21d present the same comparison, but for the concrete wall scenario. The profiles in figure 20 have been normalized to the maximum value of all plots. The Delay-Doppler patterns are obtained from data using gated FMCW signals, with a suitable gating sequence to remove the undesired wall reflection peaks as in the profiles shown in figure 20. It can be seen that the proposed wall removal technique is successful, as the positive and negative Doppler signature due to the movement of the person behind the wall are detected and the stationary wall reflections, which would appear as a strong contribution at 0 Hz Doppler, are not recorded in the pattern.

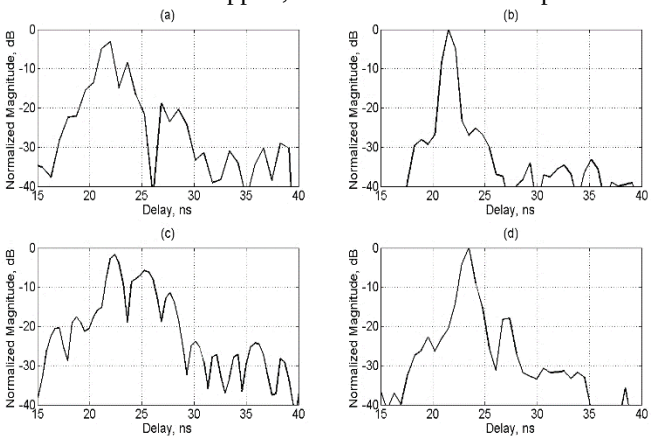

Fig. 20 FMCW delay profiles for the brick wall scenario with Vivaldi antennas (a) and with optimized patch antennas (b), and for the concrete wall scenario with Vivaldi antennas (c) and with optimized patch antennas (d)

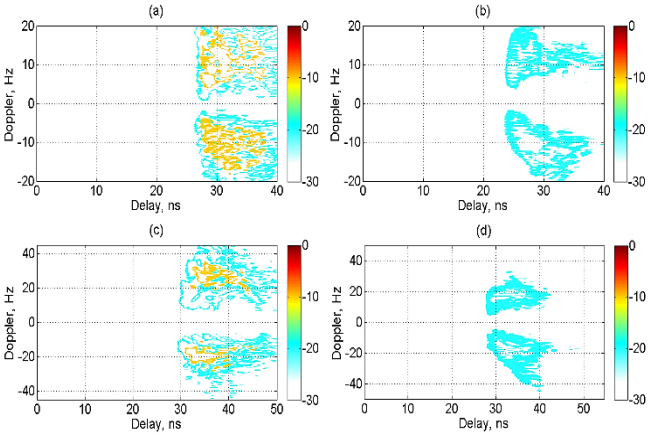

Fig. 21 FMICW Delay-Doppler for a person walking behind the brick wall with Vivaldi antennas (a) and with optimized patch antennas (b), and behind the concrete wall with Vivaldi antennas (c) and with optimized patches (d)

Both antennas can be successfully used with the developed radar system for through-wall detection, but their performance is different. Observing figure 20, it can be seen that for both scenarios the profiles related to the optimized patch have a single, cleaner lobe due to wall reflections, whereas the profiles from the Vivaldi antenna have multiple lobes which make more challenging the design of gating sequences for wall removal. The level of these side peaks is approximately 20 dB below the main peak for the patch-like antenna, but significantly higher for the Vivaldi antenna at 10 dB for the brick wall scenario and 5 dB for the concrete wall scenario. This is probably due to the broader lobe in the radiation

pattern of the Vivaldi as observed in Fig. 11, so that more reflections and clutter are detected when this antenna is used. The Vivaldi antenna gives however a stronger Doppler signal in comparison with the optimized patch, as in figure 21.

A few additional tests have been performed to investigate the effect of using antennas with different beam-widths on the collected data and on the resulting images. Besides the optimized patch-like and the Vivaldi antennas presented in this paper, low cost off-the-shelf printed log-periodic antennas were also used for comparison. These present a larger beam-width on the azimuth plane compared with the other types of antennas. An initial measurement was performed in an indoor open space environment (wide empty corridor with no wall between the radar and the target) to record the reflection from a metal plate placed at about 1.5 m in front of the antennas. Figure 22 shows the delay profiles for the three different types of antennas, using FMICW waveforms to remove the cross-talk between transmitting and receiving antennas. The target reflection peaks have been aligned for better clarity and easier comparison of the curves, and round-trip delay for the target reflection of each curve has been indicated. We can see that the peak related to the target reflection is narrow and easily detectable for the patch-like antenna, whereas it becomes slightly broader and with extra side peaks for the Vivaldi and even more for the log-periodic, probably because these antennas are also receiving clutter and unwanted reflections from the surrounding environment.

The effect of combining delay profiles with no easily recognizable target peak and with extra clutter through an imaging algorithm can be radar images containing unwanted artefacts, as we investigate in a further set of measurements. This consisted in collecting through-wall SAR data for a metal plate inside a room, behind a plastered plywood wall at about 1 m from the radar, in the same setup already discussed for figure 18. These tests were performed using the three different types of antennas and FMICW waveforms were used to remove wall reflections and the undesired cross-talk contribution. Figure 23 shows the log-scale images obtained using the BP algorithm. When the proposed patch-like antenna is used as in figure 23a, the colored spot related to the target is the strongest contribution in the image and is clearly recognizable. When the Vivaldi antenna is used, as in figure 23b, the target contribution is still easy to recognize but this colored spot is slightly smeared and offset from the actual target location, and there is an artefact appearing at about 60 cm down-range. When the log-periodic antenna is used, as in figure 23c, the target spot is present but there are other strong artefacts which may prevent the correct detection of the target. The proposed patch-like antenna provides therefore good through-wall imaging performance and has the advantage to be relatively small, easy to manufacture and low cost.

VI. Conclusion

In this paper we presented the design, manufacturing, and testing of a patch-like antenna for TTWI applications in the 0.5-2 GHz frequency range. An initial prototype has been optimized resulting in a more compact antenna with a single radiating lobe due to an additional ground plane strip. This approach may be used to increase the directivity of other printed antennas like circular patches or monopoles. The optimized patch-like antennas have been successfully used in the radar system developed at Durham University to perform an experimental campaign aimed at testing a novel wall removal technique for through-wall detection of stationary targets and of people moving. Both experimental and simulated results validate the effectiveness of the proposed wall removal technique based on FMICW waveforms in different TTWI scenarios. During the experimental campaign both optimized patch-like and conventional Vivaldi antennas have been used and their performance compared. Both antennas can be successfully used, but the patch-like appears to detect less clutter and wall reflections making easier the application of gated FMCW signals. This antenna is also smaller and made of a less expensive substrate compared with the tested antipodal Vivaldi. Further work is currently undertaken to improve the antenna design and manufacture an array to be used in conjunction with the radar system.

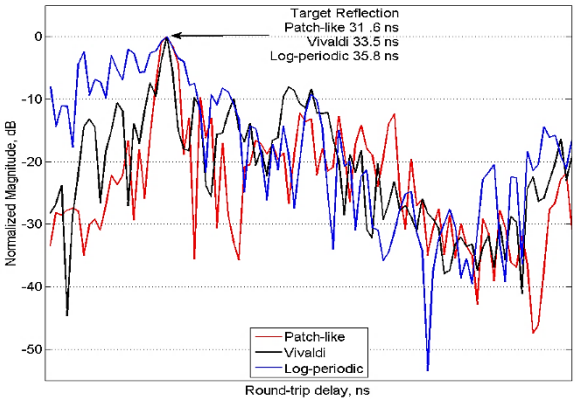

Fig. 22 FMICW normalized delay profiles for target in open space environment with three different types of antennas

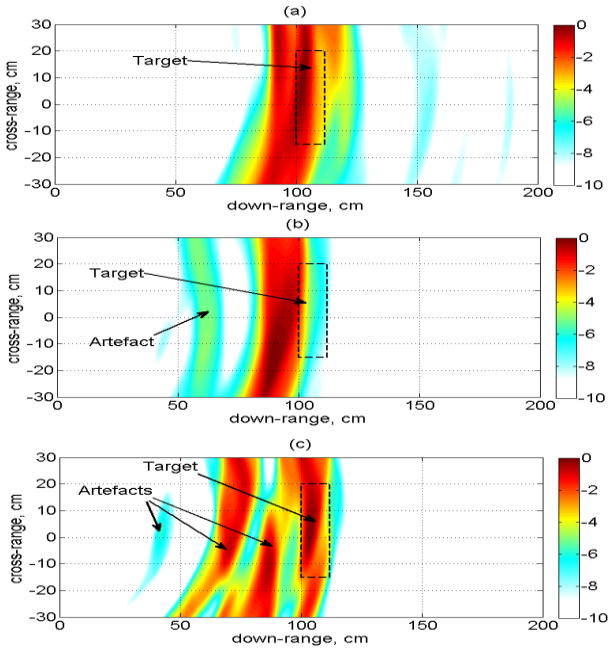

Fig. 23 FMICW Radar images in log scale for the metallic plate behind plywood wall: (a) using optimized patch-like antennas, (b) using Vivaldi antennas, and (c) using log-periodic antennas

ACKNOWLEDGMENT

The authors would like to thank Her Majesty's Government Communications Centre for sponsoring this project and the Fraunhofer IZM for hosting Francesco Fioranelli during the development of the patch-like antenna.

REFERENCES

[1] N. Maaref and P. Millot, "Array-based UWB FMCW through-the-wall radar," in *Antennas and Propagation Society International Symposium (APSURSI), 2012 IEEE*, 2012, pp. 1-2.

[2] Y. Wang, L. Quanhua, and A. E. Fathy, "Simultaneous localization and respiration detection of multiple people using low cost UWB biometric pulse Doppler radar sensor," in *Microwave Symposium Digest (MTT), 2012 IEEE MTT-S International*, 2012, pp. 1-3.

[3] T. S. Ralston, G. L. Charvat, and J. E. Peabody, "Real-time through-wall imaging using an ultrawideband multiple-input multiple-output (MIMO) phased array radar system," in *Phased Array Systems and Technology (ARRAY), 2010 IEEE International Symposium on*, 2010, pp. 551-558.

[4] G. L. Charvat, J. Goodwin, M. Tobias, J. Pozderac, and J. Peabody, "Detection algorithm implementation and measured results for a real-time, through-wall radar system using a TDM MIMO antenna array," in *Radar Conference (RADAR), 2012 IEEE*, 2012, pp. 0240-0246.

[5] F. Ahmad and M. G. Amin, "Wall clutter mitigation for MIMO radar configurations in urban sensing," in *Information Science, Signal Processing and their Applications (ISSPA), 2012 11th International Conference on*, 2012, pp. 1165-1170.

[6] M. G. Amin and F. Ahmad, "Change detection analysis of humans moving behind walls," *IEEE Trans. Aerosp. Electronic Syst*, 2013.

[7] W. Fu-Kang, H. Tzyy-Sheng, P. Kang-Chun, J. Je-Kuan, L. Jian-Yu, and C. Cheng-Chung, "Detection of concealed individuals based on their vital signs by using a see-through-wall imaging system with a self-injection-locked radar," *Microwave Theory and Techniques, IEEE Transactions on*, vol. 61, pp. 696-704, 2013.

[8] J. Sachs, M. Aftanas, S. Crabbe, M. Drutarovsky, R. Klukas, D. Kocur, *et al.*, "Detection and tracking of moving or trapped people hidden by obstacles using ultra-wideband pseudo-noise radar," in *Radar Conference, 2008. EuRAD 2008. European*, 2008, pp. 408-411.

[9] L. Biying, S. Qian, Z. Zhimin, and W. Harming, "A SFCW radar for through wall imaging and motion detection," in *Radar Conference (EuRAD), 2011 European*, 2011, pp. 325-328.

[10] R. Yu-Jiun, L. Chieh-Ping, C. Pin-Heng, and R. M. Narayanan, "Compact Ultrawideband UHF Array Antenna for Through-Wall Radar Applications," *Antennas and Wireless Propagation Letters, IEEE*, vol. 8, pp. 1302-1305, 2009.

[11] K. E. Browne, R. J. Burkholder, and J. L. Volakis, "Through-wall opportunistic sensing system utilizing a low-cost flat-panel array," *Antennas and Propagation, IEEE Transactions on*, vol. 59, pp. 859-868, 2011.

[12] J. M. Denoual, J. M. Floc'h, J. P. Mutzig, P. Massaloux, F. Ducasse, P. Minvielle, *et al.*, "Design of two flare UWB antenna dedicated to the research of alive buried victims," in *Radar Conference (EuRAD), 2010 European*, 2010, pp. 519-522.

[13] G. L. Charvat, L. C. Kempel, E. J. Rothwell, C. M. Coleman, and E. L. Mokole, "An ultrawideband (UWB) switched-antenna-array radar imaging system," in *Phased Array Systems and Technology (ARRAY), 2010 IEEE International Symposium on*, 2010, pp. 543-550.

[14] I. Munteanu, M. Timm, and T. Weiland, "It's about time," *Microwave Magazine, IEEE*, vol. 11, pp. 60-69, 2010.

[15] "IEEE Standard Test Procedures for Antennas," *ANSI/IEEE Std 149-1979*, p. 0_1, 1979.

[16] T. Dogaru and C. Le, "SAR images of rooms and buildings based on FDTD computer models," *Geoscience and Remote Sensing, IEEE Transactions on*, vol. 47, pp. 1388-1401, 2009.

[17] H. Nazli, E. Bicak, B. Turetken, and M. Sezgin, "An Improved Design of Planar Elliptical Dipole Antenna for UWB Applications," *Antennas and Wireless Propagation Letters, IEEE*, vol. 9, pp. 264-267, 2010.

[18] L. Guanghua, Z. Lingyun, T. Chaoman, and G. Lu, "A novel wide beam UWB antenna design for Through-the-Wall radar," in *Microwave and Millimeter Wave Technology (ICMMT), 2010 International Conference on*, 2010, pp. 1912-1915.

[19] N. S. Raghava, A. De, P. Arora, S. Malhotra, R. Bazaz, S. Kapur, *et al.*, "A novel patch antenna for ultra wideband applications," in *Communications and Signal Processing (ICCSP), 2011 International Conference on*, 2011, pp. 276-279.

[20] M. G. Amin, *Through-the-Wall Radar Imaging*: CRC Press, 2010.

[21] S. Salous, *Radio Propagation Measurement and Channel Modelling*: Wiley, 2013.

[22] F. Fioranelli, S. Salous, and X. Raimundo, "Frequency-Modulated Interrupted Continuous Wave as Wall Removal Technique in Through-the-Wall Imaging," *Geoscience and Remote Sensing, IEEE Transactions on*, vol. 52, pp. 6272-6283, 2014.

[23] F. Fioranelli, "Through-The-Wall Detection Using Ultra Wide Band Frequency Modulated Interrupted Continuous Wave Signals," Doctoral Thesis - Available at Durham E-Theses Online: htttp://etheses.dur.ac.uk/9432/, Durham University, 2013.

[24] G. L. Charvat, L. C. Kempel, E. J. Rothwell, C. M. Coleman, and E. Mokole, "A Through-Dielectric Radar Imaging System," *Antennas and Propagation, IEEE Transactions on*, vol. 58, pp. 2594-2603, 2010.

[25] T. Dogaru and C. Le, "Validation of Xpatch computer models for human body radar signature," Army Research Laboratory, Adelphi, MD, Tech. Rep. ARL-TR-4403, 2008.

[26] L. Chen and O. Shan, "Through-wall surveillance using ultra-wideband short pulse radar: numerical simulation," in *Industrial Electronics and Applications, 2007. ICIEA 2007. 2nd IEEE Conference on*, 2007, pp. 1551-1554.

[27] L. Hooi Been, N. Nguyen Thi Tuyet, L. Er-Ping, and T. Nguyen Duc, "Confocal microwave imaging for breast cancer detection: delay-multiply-and-sum image reconstruction algorithm," *Biomedical Engineering, IEEE Transactions on*, vol. 55, pp. 1697-1704, 2008.

[28] D. Byrne, M. O'Halloran, M. Glavin, and E. Jones, "Data independent radar beamforming algorithms for breast cancer detection," *Progress in Electromagnetic Research*, vol. 107, pp. 331-348, 2010.

[29] O'Halloran M., Glavin M., and J. E., "Performance and robustness of a multistatic mist beamforming algorithm for breast cancer detection,," *Progress In Electromagnetics Research*, vol. 105, pp. 403-424, 2010.

[30] F. Ahmad, M. G. Amin, and S. A. Kassam, "Synthetic aperture beamformer for imaging through a dielectric wall," *Aerospace and Electronic Systems, IEEE Transactions on*, vol. 41, pp. 271-283, 2005.

[31] N. Maaref and P. Millot, "Array-based ultrawideband through-wall radar: prediction and assessment of real radar abilities," *International Journal of Antennas and Propagation*, vol. 2013, p. 9, 2013.

[32] A. G. Yarovoy, X. Zhuge, T. G. Savelyev, and L. P. Ligthart, "Comparison of UWB technologies for human being detection with radar," in *Radar Conference, 2007. EuRAD 2007. European*, 2007, pp. 295-298.

[33] X. Zhuge, T. G. Savelyev, and A. G. Yarovoy, "Assessment of electromagnetic requirements for UWB through-wall radar," in *Electromagnetics in Advanced Applications, 2007. ICEAA 2007. International Conference on*, 2007, pp. 923-926.

[34] D. E. Barrick, *FM/CW radar signals and digital processing*: Environmental Research Laboratories, 1973.